Uncoupled turnover disrupts mitochondrial quality control in diabetic retinopathy

Hombrebueno, J. R., Cairns, L., Dutton, L. R., Lyons, T. J., Brazil, D. P., Moynagh, P., Curtis, T. M., & Xu, H. (2019). Uncoupled turnover disrupts mitochondrial quality control in diabetic retinopathy. *JCI insight*, *4*(23), Article e129760. Advance online publication. https://doi.org/10.1172/jci.insight.129760

Published in:
JCI insight

Document Version:
Peer reviewed version

Uncoupled turnover disrupts mitochondrial quality control in diabetic retinopathy

Jose R. Hombrebueno[1,2#], Lauren Cairns[1], Louise R. Dutton[1], Timothy J. Lyons[1,3], Derek P. Brazil[1], Paul Moynagh[1,4], Tim M. Curtis[1], Heping Xu[1]

[1]Wellcome-Wolfson Institute for Experimental Medicine, School of Medicine, Dentistry and Biomedical Sciences, Queen's University Belfast, Belfast, UK.

[2]Institute of Inflammation and Ageing, University of Birmingham, Birmingham, UK

[3]Division of Endocrinology and Diabetes, Medical University of South Carolina, Charleston, SC, USA.

[4]Institute of Immunology, Department of Biology, National University of Ireland Maynooth, Maynooth, County Kildare, Ireland

[#]Correspondence to Dr Jose Romero Hombrebueno; j.m.romero@bham.ac.uk

Institute of Inflammation and Ageing, School of Medical and Dental Sciences, University of Birmingham, Edgbaston, Birmingham, B15 2TT, UK. Phone: +44 1213713226

The authors have declared that no conflict of interest exists

Abstract

Mitochondrial quality control (MQC) is crucial for regulating central nervous system homeostasis and its disruption has been implicated in the pathogenesis of some of the most common neurodegenerative diseases. In healthy tissues, the maintenance of MQC depends upon an exquisite balance between mitophagy (removal of damaged mitochondria by autophagy) and biogenesis (*de-novo* synthesis of mitochondria). Here, we show that mitophagy is disrupted in diabetic retinopathy (DR) and decoupled from mitochondrial biogenesis during the progression of the disease. Diabetic retinas from human post-mortem donors and experimental mice exhibit a net loss of mitochondrial contents during the early stages of the disease process. Using novel diabetic mitophagy-reporter mice (*mitoQC-Ins2*^{Akita}) alongside *pMitoTimer* (a molecular clock to address mitochondrial-age dynamics), we demonstrate that mitochondrial loss arose due to an inability of mitochondrial biogenesis to compensate for diabetes-exacerbated mitophagy. However, as diabetes duration increases, Pink1-dependent mitophagy deteriorates, leading to the build-up of mitochondria primed for degradation in DR. Impairment of mitophagy during prolonged diabetes is linked with the development of retinal senescence, a phenotype that blunted hyperglycaemia-induced mitophagy in *mitoQC* primary Müller cells. Our findings suggest that normalizing mitochondrial turnover may preserve MQC and provide novel therapeutic options for the management of DR-associated complications.

Introduction

Diabetic retinopathy (DR) is a leading cause of blindness in the working-age population (1, 2). It is characterized by a progressive dysfunction of the retinal neurons, glial cells and microvasculature, leading to abnormal vessel proliferation and vascular leakage that threaten vision (3). Although the pathological hallmarks of DR are well-defined, how sustained hyperglycaemia leads to retinal neurovascular dysfunction remains to be elucidated. The pathogenesis of DR is complex and driven by a multitude of factors in addition to hyperglycaemia, including oxidative stress, dyslipidaemia and chronic para-inflammation (4). Current therapies for DR remain unsatisfactory and focus mainly on targeting the end-stages of the disease process (5). Consequently, there is an urgent need to develop new interventions, particularly those that are able to prevent the initiation and development of this condition.

A growing body of evidence suggests that mitochondrial dysfunction plays a pivotal role in the early pathogenesis of DR. For example mitochondrial DNA (mtDNA) damage, mitochondrial overproduction of reactive oxygen species (ROS) and inefficient mtDNA repair mechanisms have been implicated both in the human diabetic retina and animal models of DR (6). At the ultrastructural level, mitochondrial damage in retinal endothelial cells and neurons during DR is evidenced by the presence of vacuolated mitochondria with disruption of the lamellar cristae (7). Mitochondrial changes have also been observed in retinal cell cultures maintained under hyperglycaemia, as shown by increased mitochondrial fragmentation and reduced oxygen consumption rates (8). The accumulation of damaged mitochondria disrupts normal tissue homeostasis, and leads to exacerbated oxidative stress, energy deficits and eventually cell apoptosis (9).

The maintenance of a healthy mitochondrial network within cells depends upon mitochondrial quality control (MQC) mechanisms, which regulate the balance between mitophagy

(autophagic removal of damaged mitochondria) and biogenesis (*de novo* synthesis of mitochondria) (10). Mitophagy typically occurs in damaged mitochondria upon dissipation of the membrane potential (ψm), leading to stabilization of Pink1 at the outer mitochondrial membrane (OMM). This primes mitochondria for autophagy via activation of the E3-ubiquitin ligase Parkin (11, 12). Mitochondrial biogenesis is a dynamic process which is regulated in response to cellular metabolic demands and increases following the induction of mitophagy (13). Although several effectors are involved, PGC-1α and TFAM are critical in driving the replication of mtDNA and synthesis of proteins encoded in its genome (13).

The disruption of MQC has recently been implicated as a major cause of neurovascular pathology in a number of neurodegenerative disorders, including Parkinson's and Alzheimer's disease (14). Here, we show for the first time that mitophagy is dysregulated and uncoupled from mitochondrial biogenesis during the progression of DR.

Results

Mitochondrial contents change during the progression of DR in human and murine retinas

We first investigated mitochondrial contents in human retinas from non-diabetic subjects (ND), from people with diabetes but no retinopathy (DNR) and from people with DR, using Cox4 antibody. Overall, compared to ND, Cox4 levels were lower in DNR but elevated in DR (representative images Fig.1A). Quantitative analysis of Cox4 in specific retinal layers of DNR subjects revealed a significant reduction within synaptic processes of the outer plexiform layer (OPL) as compared to ND (Fig.1B; open-arrowheads, Fig.1C). Cox4 was also significantly reduced in the inner segments (IS) of cone-photoreceptors in DNR, (Fig.1B), further revealing mitochondrial morphological alterations in DNR subjects, including mitochondrial redistribution throughout the IS (arrow – Fig.1D) and abnormal fragmentation (arrowheads – Fig.1D). No changes were observed in Cox4 levels at the inner plexiform layer (IPL) of DNR (Fig.1B). Interestingly, Cox4 contents were not reduced in DR subjects, displaying instead a significant increase in OPL and IPL (Fig.1A-C).

To provide a basis for better understanding why mitochondrial contents shift during the course of diabetes, we examined whether these changes are recapitulated in a pre-clinical model of type-1 diabetes. Cox4 levels were investigated in 2- and 8-month hyperglycaemic *Ins2*$^{Akita/+}$ mice, which exhibit mild to severe retinal neurovascular dysfunction at these time points, respectively (15-17). Cox4 immunoblots revealed loss of mitochondrial contents in two-month hyperglycaemic *Ins2*$^{Akita/+}$ mice (Fig.2A). Immunohistochemical analysis revealed a specific decrease of Cox4 at the outer (IS-OPL) but not inner retinal layers (from inner nuclear (INL) to ganglion cell layer (GCL); Fig2.B, D). In contrast, Cox4 contents were unaffected in 8-month hyperglycaemic *Ins2*$^{Akita/+}$ mice (Fig.2A, C, E). This change of mitochondrial contents at the outer retina of *Ins2*$^{Akita/+}$ mice included photoreceptors (as assessed specifically in IS and

OPL layers - Supplemental Fig.1) and Müller cells, given the enrichment of mitochondria within glutamine synthase^{+} processes across the ONL (Supplemental Fig 2). Taken together, our data suggest that mitochondrial contents decline at the outer retina of human and *Ins2*$^{Akita/+}$ mice at the early stages of diabetes, but increase during the development of DR. This was clearly established using immunostaining against TOMM20 (a translocator of the OMM), which delineated the whole mitochondrial network at the outer retina. (Fig.2F-I).Moreover, no changes of Cox4 mRNA levels (*Cox4i1* and *Cox4i2* isoforms) were detected in 2-month and 8-months hyperglycaemic *Ins2*$^{Akita/+}$ retinas (as compared to age-matched controls, Supplemental Fig.3), suggesting that mitochondrial changes occur due to an altered mitochondrial turnover in diabetes.

Exacerbated mitophagy occurs in Ins2$^{Akita/+}$ retinas at early stages of diabetes

To determine why mitochondrial contents are reduced at the early stages of diabetes, we investigated mitochondrial biogenesis and mitophagy in 2-month hyperglycaemic *Ins2*$^{Akita/+}$ retinas. Mitochondrial biogenesis was evaluated by assessing two of the main effectors that regulate mtDNA transcription, namely, PGC-1α and TFAM (13). No significant changes in the protein levels of PGC-1α were observed in 2-month hyperglycaemic *Ins2*$^{Akita/+}$ retinas (Supplemental Fig.4A-C). TFAM immunostaining in WT mice revealed enrichment of mitochondrial nucleoids (where mtDNA is packaged into discrete mtDNA-protein complexes) (18) throughout the retina, but no significant changes in their density were observed at the IS-OPL (Supplemental Fig4.D-E). In addition, no mtDNA damage (Supplemental Fig.4G) or variations in mtDNA copy-number (Supplemental Fig.4H) were detected, supporting the absence of changes in mitochondrial biogenesis.

To unambiguously investigate mitophagy in the diabetic retina, we generated *Ins2*^{Akita} mitophagy-reporter mice (*mitoQC*$^{+/-}$*Ins2*$^{Akita/+}$), by mating *mitoQC*$^{+/+}$ (19) with *Ins2*$^{Akita/+}$ mice

(Fig.3A). In line with a recent report (19), mitophagy was mostly detected at the outer retina, as verified by high mitolysosome density (mCherry-only foci) in the IS-OPL of non-diabetic *mitoQC*$^{+/-}$*Ins2*$^{+/+}$ mice (arrowheads - Fig.3A). Diabetes amplified mitophagy at the outer retina, as indicated by a significant increase of mitolysosomes in 2-month hyperglycaemic *mitoQC*$^{+/-}$ *Ins2*$^{Akita/+}$ mice (Fig.3.A-B). These findings were further supported by analysis of Pink1 (a primary effector for the autophagic degradation of mitochondria in lysosomes (11)) in retinal lysates (Fig 3C-F). In healthy polarized mitochondria, Pink1 (FL-Pink1) shuttles to the mitochondrial matrix and is rapidly cleaved by PARL into ΔN-Pink1 (20). However, upon dissipation of Ψm, the internalization of FL-Pink1 within mitochondria is prevented and it stabilizes at the OMM, triggering the onset of mitophagy. Consistent with the increase levels of mitophagy in diabetic retinas, Pink1 levels were shifted towards its immature form, as shown by a significant elevation in the FL-Pink1/ΔN-Pink1 ratio (Fig.3 C-E). Further validation was carried out by immunohistochemical approaches. As an index of Pink1-dependent mitophagy, we assessed the percentage of Pink1^{+} puncta co-localizing with LAMP1^{+} lysosomes, which was found to increase in the outer retina of 2-month hyperglycaemic *Ins2*$^{Akita/+}$ mice (Supplemental Fig 5). Mitophagy depends on an efficient autophagic-flux and as such, this appeared to be increased at the outer retina of 2-month hyperglycaemic *Ins2*$^{Akita/+}$ mice (based on similar Lc3b^{+} autophagosomes but reduced levels of the autophagy substrate p62/SQTSM1; Supplemental Fig.6A-B, E-F, I-J) (21). Overall, our data strongly suggests that exacerbated Pink1-dependent mitophagy (together with normal mitochondrial biogenesis) underlies the reduction of mitochondrial contents at the outer retina of *Ins2*$^{Akita/+}$ mice during the early stages of diabetes.

Mitochondrial biogenesis fails to compensate for hyperglycaemia-induced mitophagy in cultured retinal Müller cells

To determine in detail how mitochondrial turnover is affected by the diabetic milieu, the interplay between mitophagy and mitochondrial biogenesis was investigated under hyperglycaemic conditions *in vitro*. Müller cells were selected for this study given a) the predominant role of mitochondrial-oxidative phosphorylation to maintain Müller basal functions (22), b) the recognized importance of Müller cells in the pathogenesis of DR (23) and c) the uniform distribution of mitochondria in Müller cells throughout the entire thickness of the neuroretina (24). To address mitophagy, we took advantage of primary Müller cells (PMCs) isolated from *mitoQC* mice. The purity of *mitoQC*-PMCs was confirmed by glutamine synthase immunostaining (Fig.4A) (25). The induction of mitophagy in *mitoQC*-PMCs was initially validated by HBSS-amino acid starvation, which significantly exacerbated the density of mitolysosomes (Fig.4A) (26). *MitoQC*-PMCs maintained in hyperglycaemia (HG; 30.5mM D-glucose) showed a significant increase of mitolysosomes, as compared to normal glucose (NG; 5.5mM D-glucose) controls (Fig.4A). Interestingly, mitophagy was also elicited by hyperosmolar changes, as observed in 30.5mM L-glucose (LG) cultures (Fig.4A). The induction of mitophagy by HG and LG was corroborated in the human Müller cell line MIO-M1, by co-localization analysis of Cox4 with $Lc3b^{+}$ autophagosomes (26) (Fig.4B). MIO-M1 cultures maintained under HG or LG for 5 consecutive days exhibited a significant increase in Cox4/Lc3b co-localization (Fig.4B), suggestive of increased mitophagy. To further substantiate this result, chloroquine was used to block autophagosome fusion with lysosomes (thus allowing the accumulation of mitochondria within autophagosomes). In line with an increased mitophagy-flux, chloroquine further exacerbated the density of Cox4/Lc3b co-localizing particles in HG and LG MIO-M1 cultures (as compared to NG chloroquine-treated cultures; Fig.4B).

Since our *in vivo* data suggested a role for Pink1 in diabetes-induced mitophagy (Fig.3C-E), we next evaluated the involvement of this pathway in HG- and LG-mediated mitophagy. Suggestive of increased Pink1-dependent mitophagy, MIO-M1 cultures maintained in HG showed a significant stabilization of FL-Pink1 (Fig.4C) and a significant elevation in the FL-Pink1/ΔN-Pink1 ratio (data not shown). Similar results were found in MIO-M1 cultures maintained in LG (Fig.4C). Interestingly, the levels of the cleaved product ΔN-Pink1 were significantly higher in LG when compared to HG cultures (Fig.4C). This result led us to hypothesize that ΔN-Pink1 levels in LG may remain constant via an increase in the number of hyperpolarized mitochondria and upregulation of PARL (which would allow the steady cleavage of FL-Pink1 within the mitochondrial matrix). As suggested, the contents of PARL (Fig.4C) and hyperpolarized mitochondria (JC-1 red fluorescence, Fig.4D) were increased in LG MIO-M1 cultures. By contrast, HG cultures, which showed a decrease in ΔN-Pink1, lacked such compensation, as reflected by the unchanged contents of PARL and hyperpolarized mitochondria (Fig.4C, D).

The above results suggest that HG and LG accelerate mitophagy, but only in the case of LG this is compensated by an increase in mitochondrial biogenesis. This idea was tested further by studying mitochondrial biogenesis. Bromodeoxyuridine (BrDU) incorporation into mtDNA (comprising the gold-standard for evaluating mitochondrial biogenesis) (27) was unchanged in MIO-M1 cultures subjected to HG (Fig.5A-B, D). This was validated at the molecular level, since the contents of molecular adaptors controlling mitochondrial biogenesis, including PGC-1α (total, Fig.5E, F - nuclear, Fig.5I-J, L) and TFAM (Fig.5E, G) remained unaltered. In comparison to HG, LG cultures exhibited increased mitochondrial biogenesis, as shown by the increased incorporation of BrDU into mtDNA (Fig.5A-D), up-regulated levels of nuclear PGC-1α (Fig.5I-L) and an apparent increase of TFAM (Fig.5E, G).

To confirm differences in the balance between mitochondrial biogenesis and mitophagy, we assessed the relative age of mitochondria. MIO-M1 cultures were transfected with *pMitoTimer* (28) and the ratio of red (old) vs green (young) fluorescent mitochondria determined (the smaller the ratio, the younger mitochondrial network). Compared to HG, LG cultures were expected to have younger mitochondrial populations, due to accelerated mitochondrial synthesis/degradation. Accordingly, LG but not HG cultures exhibited a significant decrease in *pMitoTimer* R/G ratio (Supplemental Fig.7). Collectively, these data suggest that HG activates mitophagy through a pathway involving hyperosmotic stress. In contrast, the inability of mitochondrial biogenesis to compensate for increased HG-induced mitophagy appears to result from a metabolic, rather than hyperosmotic effect. These findings may explain the loss of mitochondrial contents observed in the diabetic retina (Fig.1-2) and in MIO-M1 cultures maintained under hyperglycaemia (Cox4 immunoblots; Fig.5E, H).

Mitophagy is impaired in Ins2$^{Akita/+}$ retina at advanced stages of neurovascular dysfunction

To understand the shift towards increasing mitochondrial contents at advanced stages of DR (Fig.1-2), we investigated mitochondrial biogenesis and mitophagy in 8-month hyperglycaemic *Ins2$^{Akita/+}$* mice. In contrast to younger ages, the mitochondrial biogenesis machinery was shown to be impaired at this stage, as indicated by a decrease in TFAM protein levels and of TFAM^{+}-mitochondrial nucleoids at the IS-OPL (Fig.6D-F), substantial mtDNA damage (Fig.6G) and reduced mtDNA copy number (Fig.6H). Upregulated mitochondrial biogenesis cannot therefore explain the normalization of Cox4 levels observed in 8-month hyperglycaemic *Ins2$^{Akita/+}$* mice.

Importantly, the analysis of mitophagy revealed a significant decrease of mitolysosomes at the outer retina of 8-month hyperglycaemic *mitoQC$^{+/-}$Ins2$^{Akita/+}$* mice (as compared to non-diabetic *mitoQC$^{+/-}$Ins2$^{+/+}$*, Fig.7A-B). However, FL-Pink1 stabilization and Parkin levels were

strikingly increased (Fig.7C-E), suggesting that Pink1-primed mitochondria are ineffectively cleared and accumulate in the retina at advanced stages of diabetes. This was further evidenced by a significant accumulation of ubiquitin and p62 in the mitochondria of photoreceptor IS (however, this was not observed in younger diabetic stages with competent mitophagy; Supplemental Fig 8). Autophagy adaptors were found also to accumulate at the outer retina, indicated by increased Lc3b^{+} autophagosomes and p62/SQTSM1 (Supplemental Fig.6C-D, G-H, I-J). Importantly, the gene transcripts of those mitophagy (*Pink1, Park2*) (Fig.7F-G) and autophagy (*Map1lc3b*, *sqstm1*) (Supplemental Fig.6K) effectors were unchanged in the diabetic retina at this stage, suggesting their accumulation at the protein level due inefficient autophagy/mitophagy. To confirm this hypothesis, we evaluated the levels of mitochondria entering a) autophagosomes (Cox4/Lc3b co-localization) and b) Pink1-dependent mitophagy (Pink1/LAMP1 co-localization). The levels of mitochondria co-localizing with Lc3b^{+} autophagosomes were significantly increased at the outer retina (Supplemental Fig.9A, C); however, their degradation by lysosomes appeared impaired as the levels of Pink1 co-localizing with LAMP1 were not elevated (Supplemental Fig.9B, D). Thus, disruption of Pink1-mitophagy may contribute to the build-up of mitochondria primed for degradation during advanced stages of DR.

Disruption of mitophagy in the diabetic retina is associated with increased cellular senescence

Mitophagy is known to be perturbed in senescent cells, which may result in the accumulation of damaged mitochondria (29, 30). Hence, we finally investigated whether the impairment of mitophagy at advanced stages of diabetes is associated with a senescent retinal phenotype. In support of this, up-regulated SA-β-Gal activity (31) was observed at the outer retina of 8-month but not 2-month hyperglycaemic *Ins2*$^{Akita/+}$ mice (Fig.8A-C). To further understand whether diabetes-induced mitophagy may be impaired by cellular senescence, replicative, non-chemical

senescence was induced in *mitoQC*-PMCs (by continuous passage (P) of the cells until P5-P6) and mitophagy elicited by HG, LG or HBSS. Senescence was confirmed in P5-P6 *mitoQC*-PMCs cultures, as shown by exacerbated SA-β-Gal activity, an enlarged/flat morphology and negligible nuclear-levels of the proliferative marker Ki67 (Fig.8D). In contrast to earlier passages, mitophagy was not elicited in senescent *mitoQC*-PMCs following treatments with HG, LG or HBSS (Fig8.E-F). Hence, the premature senescence of cells at the outer retina may explain the disruption of mitophagy at advanced stages of diabetes.

Discussion

Our study has demonstrated how MQC becomes dysregulated in the retina during the progression of diabetes. Early stages were characterised by the net loss of mitochondrial contents at the outer retina, as mitochondrial biogenesis was unable to compensate for increased diabetes-induced mitophagy. However, mitophagy was shown to decline with diabetes duration, shifting mitochondrial contents towards normal values. Our data further suggest that mitophagy may be disrupted by senescence at advanced stages of diabetes.

A key observation from our study involves the increased mitophagy of the diabetic retina, which particularly affected outer retinal layers. As observed for MIO-M1 cultures maintained under LG, the increased mitophagy of the diabetic retina may arise due to increased hyperosmotic stress. Although the mechanisms remain unclear, changes in cellular osmolarity have been reported to influence the turnover of mitochondria (32). Nonetheless, additional insults might also be responsible for the dysregulation of mitophagy in the retina at the early stages of diabetes. Photoreceptors are highly metabolic cells, exhibiting the highest contents of mitochondria in the retina (as they rely on oxidative-phosphorylation to support vision) (33). Since this process generates large amounts of ROS capable of damaging mitochondria, a greater demand for ROS-mediated mitophagy (34) at the outer retina might be expected. Previous studies have demonstrated increased mitochondrial-superoxide production in the diabetic retina (35) which, in turn, could exacerbate the mitophagy demands. The overproduction of mitochondrial-ROS in cell cultures exposed to hyperglycaemia is also well documented (36, 37). Further studies are therefore warranted to more precisely understand the factors that contributed to increased mitophagy in the diabetic retina.

Our study suggested that Pink1 may contribute to retinal mitophagy; however as recently suggested the rate of mitophagy in the retina was shown to be unaffected in *Pink1*$^{-/-}$ mice (19).

Although this highlights a dispensable role for Pink1 in physiological conditions, our study supports an important role of this pathway to drive mitophagy in the diabetic context. Nonetheless, other pathways including BNIP3L/NIX or TXNIP might also be important for orchestrating mitophagy in diabetes (36, 38). Further investigations are thus needed to precisely map the importance of the different mitophagy pathways in the diabetic retina, which extends beyond the scope of this current study.

As shown in *Ins2*$^{Akita/+}$ mice and in hyperglycaemic MIO-M1 cultures, mitochondrial biogenesis was unable to compensate for increased diabetes-induced mitophagy. This lack of compensation is most likely explained by metabolic (rather than hyperosmotic) stress, since LG cultures counteracted mitochondrial degradation through upregulation of biogenesis. Since the biogenesis machinery appeared unaltered in 2-months hyperglycaemic *Ins2*$^{Akita/+}$ mice, it remains unclear why mitophagy is not appropriately counteracted at the early stages of diabetes. Previous investigations have suggested the dysregulation of mitochondrial biogenesis in the diabetic retina, may result, at least in part, due to damage to mtDNA replication systems (39); however, this hallmark was observed in *Ins2*$^{Akita/+}$ mice only at the advanced stages of the disease. The dysregulation of mitochondrial biogenesis in the hyperglycaemic context may have important pathophysiological consequences, including bio-energetic deficits due a net-loss of mitochondrial mass. On the other hand, the reduction of mitochondrial mass may reflect an attempt to decrease the overproduction of mitochondrial-ROS in the diabetic retina and/or minimize pathophysiological effects associated with the accumulation of damaged mitochondria, such as cGAS-STING mediated pro-inflammatory insult and activation of intrinsic mitochondrial-apoptotic pathways (40).

A reduction in the rate of mitophagy was observed at the outer retina in advanced stages of diabetes. The disruption of MQC through the impairment of mitophagy has emerged as major cause of Central Nervous System degeneration, since it may lead to the build-up of oxidized

mitochondria incompatible with tissue homeostasis (14). Hence, it is not surprising that impaired mitophagy in *Ins2*$^{Akita/+}$ mice was associated with mtDNA damage but also with a disease stage where advanced neurovascular degeneration has been reported (15, 17). Whether the reduction in the rate of mitophagy at advanced stages arises due to failure of autophagy, mitophagy or both needs further investigation. Previous studies supported the dysregulation of autophagy in the diabetic retina, either suggesting an increase (41) or a deficiency (42) in the flux. Our study concurs with both observations depending on the duration of diabetes examined. In contrast to 2-month hyperglycaemic *Ins2*$^{Akita/+}$ mice where autophagy appears to be coupled with increased mitophagy-flux, at advanced stages of the disease, the accumulation of Lc3b^{+} autophagosomes and p62/SQTSM1 may indicate ineffective autophagy (21). This could arise due to a deficit of cargo degradation in lysosomes, since the levels of mitochondria entering autophagosomes were increased.

We further propose that premature senescence of the outer retina may play an important role in the disruption of MQC, which may shift mitochondrial contents to higher levels at advanced stages of DR. In agreement with this, the accumulation of dysfunctional mitochondria is a well-known hallmark of senescent cells (30). At present, the mechanisms initiating cellular senescence in the diabetic retina remain uncertain. The increase of autophagic-flux from the early stages could potentially facilitate the process of senescence (43). Moreover, the dysregulation of MQC due to inefficient mitophagy may also contribute to this process (30). Aside from these factors, other different stressors such as genotoxic or oxidative insult could be relevant (44). Regardless of its origin, the senescence of the diabetic retina may have important pathological implications, such as the development of senescence-associated secretory phenotype (SASP), associated with an exacerbated secretion of pro-inflammatory mediators (45).

In summary, our study provides novel insights into the pathobiology of DR which may be therapeutically relevant for the early and advanced stages of the disease. Therapies aimed at counteracting increased diabetes-induced mitophagy through stimulating mitochondrial biogenesis may be important during the early stages. However, this strategy could involve a risk when the efficiency of mitophagy decreases (i.e. at more advanced stages), which may worsen the accumulation of damaged mitochondria in the diabetic retina. Whilst promoting mitophagy at these stages appears reasonable, future studies will determine the suitability of those therapies for the management of DR.

Methods

Animals

Male heterozygous *Ins2*$^{Akita/+}$ mice of C57BL/6J background (originally purchased from Jackson Laboratory, Bar Harbor, USA) and age-matched non-diabetic siblings (WT) were used in the study. The *Ins2*$^{Akita/+}$ mice develops severe hyperglycaemia (above 550 mg/dL (or) 30.5mM) by 4-weeks of age (46). *Ins2*^{Akita} mitophagy-reporter mice (*mitoQC*$^{+/-}$*Ins2*$^{Akita/+}$) was generated by mating *mitoQC*$^{+/+}$ females (kindly provided by Dr. Ian Ganley – University of Dundee, Dundee, UK) with *Ins2*$^{Akita/+}$ males. The diabetic phenotype in the resultant male offspring was corroborated by the levels of glucose (above 550 mg/dL (or) 30.5mM) and HbA1c (diabetic *mitoQC*$^{+/-}$*Ins2*$^{Akita/+}$ had 113.5 ± 4.6 mmol/mol; non-diabetic *mitoQC*$^{+/-}$*Ins2*$^{+/+}$ siblings had 29.7 ± 1.9 mmol/mol). Detection of the *mitoQC* knockin allele (*mCherry-GFP-mtFIS1*$^{101–153}$) was determined by PCR (47).

rtPCR

Total RNA was isolated from *Ins2*$^{Akita/+}$ and age-matched WT retinas (n=6-8 retinas/group) using the RNeasy Mini Kit (Qiagen) and rtPCR performed using SYBR-Green Master in a Light-Cycler 480 system (Roche-Diagnostics GmbH). The relative expression of target genes (Supplemental Table 1) was normalized to *18s*.

Mitochondrial copy number

Total DNA from *Ins2*$^{Akita/+}$ and age-matched WT retinas (n=7-10 retinas/group) was extracted using the DNeasy Blood & Tissue Kit (Qiagen) and rtPCR performed using specific primers (Supplemental Table 1) to detect *mMITO* and *cytochrome-c oxidase subunit II* (*CoII*) as markers for mtDNA, and *18s*, for nuclear DNA (nDNA). The mtDNA/nDNA ratio was used as measurement of mtDNA copy number.

mtDNA damage

Total DNA from *Ins2*$^{Akita/+}$ and age-matched WT retinas (n=7-10 retinas/group) was amplified by PCR using specific primers (Supplemental Table 1) for long (10.1 Kb) and short (116 pb) mtDNA regions (48). Long and short amplification products were respectively separated in 1% and 2% agarose gels and the intensity of SYBR_Safe DNA blots quantified using FIJI software (National Institutes of Health, Bethesda, USA). The relative amplification of the long PCR product was normalized to the short product; a reduction in the amplification ratio was indicative of increased mtDNA damage (48).

Intravitreal injection of chloroquine

Autophagy flux in the retina was blocked via intravitreal administration of 1µl chloroquine (500 µM) in three-month old WT mice. Injections were performed as previously reported (49). Twenty four hours following chloroquine administration mouse eyes were collected and processed for immunohistochemistry.

Immunohistochemistry

Human retinas: Age-matched human retinas from diabetic and non-diabetic individuals were obtained post-mortem from the National Disease Research Interchange (Philadelphia) as described (41). The groups were categorized as non-diabetic (n=3 donors), diabetes with no retinopathy (n=5 donors; of which type-1 diabetes n=3, type-2 diabetes n=2), diabetes with retinopathy (n=2 donors; type-2 diabetes, non-proliferative diabetic retinopathy). Following deparaffinization, retinal sections were immersed (1h) in Antigen Retrieval Buffer (EDTA, pH 8.0) at 60°C. Sections were then rinsed in PBS and incubated overnight (4°C) with Cox4 and cone-arrestin antibodies (Supplemental Table 2) as previously described (50); *Mouse retinas:*

Eyes were dissected, fixed in 2% paraformaldehyde and processed for immunohistochemistry (Supplemental Table 2) as previously described (50).

Cell culture

The human Müller cell line Moorfields/Institute of Ophthalmology- Müller 1 (MIO-M1) was obtained from the UCL Institute of Ophthalmology, London, UK (51). PMCs from *mitoQC*$^{+/+}$ mice were isolated and cultured as previously described (25). PMCs were used for experiments from P2 until P6, where most cells showed a senescence phenotype. Cultures were maintained in DMEM (containing 10% FCS, 100U/mL penicillin-streptomycin) and supplemented with 5.5mM D-glucose (NG), 30.5mM D-glucose (HG) or 30.5mM L-glucose (25mM LG + 5.5mM NG) for five days. The selection of 30.5mM D-glucose was based on the levels of hyperglycaemia found in the plasma of *Ins2*$^{Akita/+}$ mice. For mitophagy-induced aminoacid starvation, cultures were maintained in HBSS (16h). Autophagy-flux was blocked with 100μM chloroquine (12h). Endpoint experiments were performed in 70-80% confluent cultures. No mycoplasma was detected in the cell cultures

Immunocytochemistry

Cells were fixed in 2% paraformaldehyde, rinsed in PBS and blocked (3% BSA 0.1% TritonX-100 PBS). Cells were then incubated overnight (4°C) with primary antibodies (Supplemental Table 2) diluted in 3% BSA 0.05% Tween-20 PBS. Following incubation, cells were probed (1h) with fluorophore-conjugated secondary antibodies at room-temperature.

Western blotting

Retinas and MIO-M1 cells were lysed in RIPA buffer with protease and phosphatase inhibitors cocktails (Sigma-Aldrich). Protein samples (10-20μg) were run on 7.5%, 10% or 12% (w/v) SDS-PAGE gel and samples immunoblotted for primary antibodies (Supplemental Table 2).

Immunoblots (obtained from 3 biological replicates) were quantified by densitometry and protein expressions normalized to β-actin or α-tubulin levels.

pMitoTimer transfections

pMitoTimer incorporates a fluorescent timer-reporter to mitochondria (*pDsRed2-Mito*) that fluoresces GFP when newly-synthetized and irreversibly shifts to red spectrum (Ex/Em 558/583nm) over time (28). MIO-M1 cells were incubated (12h) with a mixture of 50ng plasmid-DNA and 0.15µl endofectin (GeneCopoeia) in Opti-MEM (Thermo-Fisher). Cells were then maintained in NG, HG or LG and fixed for microscopy.

JC-1 dye staining

Mitochondrial membrane potential was assessed by ratiometric analysis of JC-1 (Thermo-Fisher). Following NG, HG or LG treatment, MIO-M1 cultures were supplemented with 0.5µg/ml JC-1 (30 min at 37ºC) and returned to DMEM for microscopy. Positive controls were supplemented for 16h with carbonyl cyanide m-chlorophenylhydrazone (CCCP, 20 µM) to uncouple mitochondria.

Immunolabelling BrDU-DNA

Following NG, HG or LG treatment, cultures were supplemented (12h) with 10µM BrdU (Thermo-Fisher) and fixed. Cells were then rinsed in PBS and the DNA denatured (20 min) with 0.5M HCl. Cells were washed with PBS and processed for anti-BrDU immunocytochemistry.

SA-β-Gal activity

Retinal cryosections obtained from *Ins2*$^{Akita/+}$ and WT mice (n=6 eyes/group) and *mitoQC*-PMCs cultures (P2-P3 and P5-P6) were processed following manufacturer's instructions of the Senescence Detection Kit (Abcam)

Confocal morphometry

Confocal images were acquired under constant photomultiplier settings (C1-Nikon_Eclipse TE200-U) and analysed using FIJI software. To avoid any bias during imaging, retinal regions were selected based on the DAPI nuclear signal and invariably, from middle-centre eccentricities. For cell cultures, images were selected from the same cardinal points of the wells using brightfield imaging.

Cox4 levels in human retinal sections: Images (2 retinal sections/eye; 8 images/section) were used to quantify the mean fluorescence intensity (MFI) of Cox4. For this purpose, mean luminance values (average brightness per pixel) were calculated from manually traced areas, including a) IS of cone-photoreceptors (identified by cone-arrestin immnoreactivity), b) OPL and c) IPL. Background was acquired from a vacant area of the labeled section and subtracted from the raw images to eliminate background noise. The technical replicates (n=16 for each eye) were used for statistical analysis.

MFI in mouse retinas: Images (n=4-5 eyes/group; 2 retinal sections/eye; 4 images/section) were used to quantify the MFI values of Cox4, PGC-1α, Lc3b and p62/SQTSM1 in WT and *Ins2*$^{Akita/+}$ mice. Measurements were obtained a) from the photoreceptor IS to the OPL (referred as the outer retina) and b) from the INL to the GCL (referred as the inner retina). MFI values were averaged for each eye.

Ubiquitin in mitochondria of photoreceptor inner segments: Images (n=5-6 eyes/group; 2 retinal sections/eye; 4 images/section) were used to delineate mitochondrial ROIs ($Fis1^+$ area) in photoreceptor IS. The MFI of ubiquitin immunostaining was then assessed in mitochondrial ROIs. MFI values were averaged for each eye.

Quantification of $TFAM^+$mitochondrial nucleoids and $TOMM20^+$ mitochondria at the outer retina: Mitochondrial nucleoids and $TOMM20^+$ mitochondria were quantified in confocal retinal images (n=5-8 eyes/group; 2 retinal sections/eye; 4 images/section) by threshold image-binarization of $TFAM^+$ or $TOMM20^+$ particles at the IS-OPL (constant values were applied for all groups) and their number obtained by particle analysis in FIJI. Mitochondrial nucleoid and $TOMM20^+$ mitochondrial values were then normalized to the outer retinal area analysed. Values were averaged for each eye.

Quantification of mitolysosomes (mCherry-only foci) at the outer retina: The total mitolysosome number in confocal retinal images (n=4-8 eyes/group, 2 retinal sections/eye; 4 images/section) at the outer retina (IS-OPL) was determined by the subtraction of GFP signal from mCherry using the 'image calculator' plugin of FIJI. This was followed by threshold image-binarization of mitolysosomes (constant values were applied for all groups) and the total number obtained by particle analysis. Mitolysosome number was then normalized to the outer retinal area analysed. Values were averaged for each eye.

SA-β-Gal in mouse retinas: Images (n=6 eyes/group; 2 retinal sections/eye; 4 images/section) were inverted and transformed into 32-bit colour to quantify the intensity of SA-β-Gal staining in WT and $Ins2^{Akita/+}$ mice. Measurements obtained from the IS were averaged for each eye.

Quantification of mitolysosomes in mitoQC-PMCs: The total mitolysosome area in individual cells was determined by the subtraction of GFP signal from mCherry using the *'image*

calculator' plugin of FIJI. This was followed by threshold image-binarization of mitolysosomes (constant values were applied for all groups) and the total area (μm^2) obtained by particle analysis. Values (P2-P3 cells, n=3-5 biological replicates per group; P5-P6 cells, n=2 biological replicates and 4 technical replicates per group) were normalized to the cellular area.

BrDU incorporation in mtDNA: The cytoplasmic area of each individual cell was manually traced, inverted and duplicated for analysis. The BrDU positive-area was then delineated by threshold image-binarization (using constant values for all groups) and the total area (μm^2) obtained by particle analysis. Values were normalized to the cellular area. At least 70 cells (obtained from n=3 biological replicates) were analysed. The specificity of BrDU within mitochondria was validated by co-staining with TOMM20 (data not shown).

Ratiometric analysis of pMitoTimer: Red- and GFP-fluorescent signals were merged and *pMitoTimer* ROIs obtained by threshold image-binarization and particle analysis. Red- and GFP-fluorescent MFIs were then obtained from the *pMitoTimer* ROIs and the Red to Green ratio calculated in each image. Cells obtained from n=2 biological replicates (5 technical replicates per group) were analysed.

Co-localization analysis in retina: Images (n=5 eyes/group; 2 retinal sections/eye; 2 images/section) were processed for co-localization analysis using the *Intensity Correlation Analysis* of the WCIF-ImageJ module (52). The total co-localizing area (μm^2) was then obtained by threshold image-binarization and particle analysis of the generated *+ves stack* (which shows all positive co-localizing pixels). The percentage of Cox4 or Pink1, respectively co-localized with Lc3b or LAMP1, was determined as = *[total co-localizing area]*100 / [Cox4 (or) Pink1 area]*. For each eye, values were averaged. Pink1 antibody was validated using *MitoQC*$^{+/+}$*Pink1*$^{-/-}$ mouse eyes (kindly provided by Dr. Ian Ganley,

University of Dundee, Dundee, UK) (Supplemental Fig.10A). Pink1, Lc3b and LAMP1 antibodies were further validated for immunohistochemistry via intravitreal injection of chloroquine in mouse eyes (Supplemental Fig.10B-D).

Co-localization analysis in MIO-M1 cells: The total co-localizing area between Cox4 and Lc3b (calculated as above) was normalized to the cell area. Data was then referred as fold changes to NG. At least 70 cells (obtained from n=3 biological replicates) were analysed.

Statistics

In each age-group, the difference between two means was analysed using two-sided unpaired Student's *t*-test and One-way ANOVA (followed by Bonferroni's post-hoc analysis) used for comparisons with more than two groups (GraphPad-Prism). To compare the difference between two means by immunohistochemical morphometry, sample size was adjusted to n=4-9 eyes in each mouse group based on an 80% power and a 5% significant level. Significant out-layers were discarded using Grubbs' test (alpha=0.05). Data were expressed as mean ± SEM. $p<0.05$ was considered statistically significant.

Study approval

The study was approved by the Ethics Committee at the Queen's University of Belfast and Institutional Review Board at the University of Oklahoma Health Sciences Centre (OUHSC). Human studies were conducted according to the Declaration of Helsinki principles and written informed consent was received from participants prior to inclusion in the study. All animal procedures were approved by Ethical Review Body (AWERB) and authorized under the UK Animals (Scientific Procedures) Act 1986. Animal use conformed to the standards in the Association for Research in Vision and Ophthalmology (ARVO) Statement for the Use of Animals in Ophthalmic and Vision Research and with European Directive 210/63/EU.

Author Contributions

J.R.H. conceived and designed the experiments with input from T.M.C, P.M, H.X; J.R.H., L.C. and L.D. performed the experiments; J.R.H. and L.C. analysed the data; T.J.L. contributed with the human retinal samples and D.P.B. and H.X. contributed with reagents/materials; J.R.H. and T.M.C. wrote and edited the manuscript with input from all other authors. J.R.H. supervised the project.

Acknowledgments

This work was supported by an Early Career Investigator Award from Fight for Sight (1842/1843) to J.R.H.

Special thanks to Dr Ian G. Ganley (University of Dundee) for providing us with the *mitoQC* mice and *mitoQC* Pink1 KO eyes and Professor Astrid Limb (University College London) for providing the MIO-M1 cell line. We thank the eye donors for their inestimable contribution to DR research

References

1. Klein BE. Overview of epidemiologic studies of diabetic retinopathy. *Ophthalmic epidemiology.* 2007;14(4):179-83.
2. Lee R, Wong TY, and Sabanayagam C. Epidemiology of diabetic retinopathy, diabetic macular edema and related vision loss. *Eye and vision.* 2015;2:17.
3. Gardner TW, Antonetti DA, Barber AJ, LaNoue KF, Levison SW, and Grp PSRR. Diabetic retinopathy: More than meets the eye. *Surv Ophthalmol.* 2002;47:S253-S62.
4. Zhang W, Liu H, Rojas M, Caldwell RW, and Caldwell RB. Anti-inflammatory therapy for diabetic retinopathy. *Immunotherapy.* 2011;3(5):609-28.
5. Evans JR, Michelessi M, and Virgili G. Laser photocoagulation for proliferative diabetic retinopathy. *The Cochrane database of systematic reviews.* 2014;11:CD011234.
6. Kowluru RA, and Mishra M. Oxidative stress, mitochondrial damage and diabetic retinopathy. *Biochimica et biophysica acta.* 2015;1852(11):2474-83.
7. Zhong Q, and Kowluru RA. Diabetic retinopathy and damage to mitochondrial structure and transport machinery. *Investigative ophthalmology & visual science.* 2011;52(12):8739-46.
8. Tien T, Zhang J, Muto T, Kim D, Sarthy VP, and Roy S. High Glucose Induces Mitochondrial Dysfunction in Retinal Muller Cells: Implications for Diabetic Retinopathy. *Investigative ophthalmology & visual science.* 2017;58(7):2915-21.
9. Van Houten B, Hunter SE, and Meyer JN. Mitochondrial DNA damage induced autophagy, cell death, and disease. *Frontiers in bioscience.* 2016;21:42-54.
10. Meyer JN, Leuthner TC, and Luz AL. Mitochondrial fusion, fission, and mitochondrial toxicity. *Toxicology.* 2017;391:42-53.
11. Jin SM, and Youle RJ. PINK1-and Parkin-mediated mitophagy at a glance. *Journal of cell science.* 2012;125(4):795-9.
12. Ding WX, and Yin XM. Mitophagy: mechanisms, pathophysiological roles, and analysis. *Biological chemistry.* 2012;393(7):547-64.
13. Austin S, and St-Pierre J. PGC1alpha and mitochondrial metabolism--emerging concepts and relevance in ageing and neurodegenerative disorders. *Journal of cell science.* 2012;125(Pt 21):4963-71.
14. Fivenson EM, Lautrup S, Sun N, Scheibye-Knudsen M, Stevnsner T, Nilsen H, et al. Mitophagy in neurodegeneration and aging. *Neurochem Int.* 2017;109:202-9.
15. Barber AJ, Antonetti DA, Kern TS, Reiter CE, Soans RS, Krady JK, et al. The Ins2Akita mouse as a model of early retinal complications in diabetes. *Investigative ophthalmology & visual science.* 2005;46(6):2210-8.
16. Han Z, Guo J, Conley SM, and Naash MI. Retinal angiogenesis in the Ins2(Akita) mouse model of diabetic retinopathy. *Investigative ophthalmology & visual science.* 2013;54(1):574-84.
17. Hombrebueno JR, Chen M, Penalva RG, and Xu H. Loss of synaptic connectivity, particularly in second order neurons is a key feature of diabetic retinal neuropathy in the Ins2Akita mouse. *PloS one.* 2014;9(5):e97970.
18. Lee SR, and Han J. Mitochondrial Nucleoid: Shield and Switch of the Mitochondrial Genome. *Oxid Med Cell Longev.* 2017;2017:8060949.
19. McWilliams TG, Prescott AR, Montava-Garriga L, Ball G, Singh F, Barini E, et al. Basal Mitophagy Occurs Independently of PINK1 in Mouse Tissues of High Metabolic Demand. *Cell metabolism.* 2018;27(2):439-+.
20. Deas E, Plun-Favreau H, Gandhi S, Desmond H, Kjaer S, Loh SHY, et al. PINK1 cleavage at position A103 by the mitochondrial protease PARL. *Human molecular genetics.* 2011;20(5):867-79.
21. Yoshii SR, and Mizushima N. Monitoring and Measuring Autophagy. *International journal of molecular sciences.* 2017;18(9).

22. Augustine J, Pavlou S, O'Hare M, Harkin K, Stitt A, Curtis T, et al. Characterization of a Spontaneously Immortalized Murine Muller Glial Cell Line QMMuC-1. *Investigative ophthalmology & visual science.* 2018;59(3):1666-74.
23. Coughlin BA, Feenstra DJ, and Mohr S. Muller cells and diabetic retinopathy. *Vision research.* 2017;139:93-100.
24. Germer A, Biedermann B, Wolburg H, Schuck J, Grosche J, Kuhrt H, et al. Distribution of mitochondria within Muller cells--I. Correlation with retinal vascularization in different mammalian species. *Journal of neurocytology.* 1998;27(5):329-45.
25. Liu X, Tang L, and Liu Y. Mouse Muller Cell Isolation and Culture. *Bio-protocol.* 2017;7(15).
26. Allen GF, Toth R, James J, and Ganley IG. Loss of iron triggers PINK1/Parkin-independent mitophagy. *EMBO reports.* 2013;14(12):1127-35.
27. Lentz SI, Edwards JL, Backus C, McLean LL, Haines KM, and Feldman EL. Mitochondrial DNA (mtDNA) Biogenesis: Visualization and Duel Incorporation of BrdU and EdU Into Newly Synthesized mtDNA In Vitro. *J Histochem Cytochem.* 2010;58(2):207-18.
28. Laker RC, Xu P, Ryall KA, Sujkowski A, Kenwood BM, Chain KH, et al. A Novel MitoTimer Reporter Gene for Mitochondrial Content, Structure, Stress, and Damage in Vivo. *J Biol Chem.* 2014;289(17):12005-15.
29. Wiley CD, Velarde MC, Lecot P, Liu S, Sarnoski EA, Freund A, et al. Mitochondrial Dysfunction Induces Senescence with a Distinct Secretory Phenotype. *Cell metabolism.* 2016;23(2):303-14.
30. Korolchuk VI, Miwa S, Carroll B, and von Zglinicki T. Mitochondria in Cell Senescence: Is Mitophagy the Weakest Link? *Ebiomedicine.* 2017;21:7-13.
31. Dimri GP, Lee XH, Basile G, Acosta M, Scott C, Roskelley C, et al. A Biomarker That Identifies Senescent Human-Cells in Culture and in Aging Skin in-Vivo. *Proceedings of the National Academy of Sciences of the United States of America.* 1995;92(20):9363-7.
32. May AI, Devenish RJ, and Prescott M. The many faces of mitochondrial autophagy: making sense of contrasting observations in recent research. *International journal of cell biology.* 2012;2012:431684.
33. Wong-Riley MT. Energy metabolism of the visual system. *Eye Brain.* 2010;2:99-116.
34. Baldelli S, Aquilano K, and Ciriolo MR. PGC-1 alpha buffers ROS-mediated removal of mitochondria during myogenesis. *Cell death & disease.* 2014;5.
35. Du Y, Veenstra A, Palczewski K, and Kern TS. Photoreceptor cells are major contributors to diabetes-induced oxidative stress and local inflammation in the retina. *Proceedings of the National Academy of Sciences of the United States of America.* 2013;110(41):16586-91.
36. Devi TS, Somayajulu M, Kowluru RA, and Singh LP. TXNIP regulates mitophagy in retinal Muller cells under high-glucose conditions: implications for diabetic retinopathy. *Cell death & disease.* 2017;8(5):e2777.
37. Yu T, Robotham JL, and Yoon Y. Increased production of reactive oxygen species in hyperglycemic conditions requires dynamic change of mitochondrial morphology. *Proceedings of the National Academy of Sciences of the United States of America.* 2006;103(8):2653-8.
38. Esteban-Martinez L, Sierra-Filardi E, McGreal RS, Salazar-Roa M, Marino G, Seco E, et al. Programmed mitophagy is essential for the glycolytic switch during cell differentiation. *Embo Journal.* 2017;36(12):1688-706.
39. Santos JM, Tewari S, Goldberg AF, and Kowluru RA. Mitochondrial biogenesis and the development of diabetic retinopathy. *Free radical biology & medicine.* 2011;51(10):1849-60.
40. Li T, and Chen ZJJ. The cGAS-cGAMP-STING pathway connects DNA damage to inflammation, senescence, and cancer. *J Exp Med.* 2018;215(5):1287-99.
41. Fu D, Yu JY, Yang S, Wu M, Hammad SM, Connell AR, et al. Survival or death: a dual role for autophagy in stress-induced pericyte loss in diabetic retinopathy. *Diabetologia.* 2016;59(10):2251-61.

42. Lopes de Faria JM, Duarte DA, Montemurro C, Papadimitriou A, Consonni SR, and Lopes de Faria JB. Defective Autophagy in Diabetic Retinopathy. *Investigative ophthalmology & visual science.* 2016;57(10):4356-66.
43. White E, and Lowe SW. Eating to exit: autophagy-enabled senescence revealed. *Genes & development.* 2009;23(7):784-7.
44. Ben-Porath I, and Weinberg RA. The signals and pathways activating cellular senescence. *Int J Biochem Cell B.* 2005;37(5):961-76.
45. Coppe JP, Desprez PY, Krtolica A, and Campisi J. The Senescence-Associated Secretory Phenotype: The Dark Side of Tumor Suppression. *Annu Rev Pathol-Mech.* 2010;5:99-118.
46. Yoshioka M, Kayo T, Ikeda T, and Koizumi A. A novel locus, Mody4, distal to D7Mit189 on chromosome 7 determines early-onset NIDDM in nonobese C57BL/6 (Akita) mutant mice. *Diabetes.* 1997;46(5):887-94.
47. McWilliams TG, Prescott AR, Allen GFG, Tamjar J, Munson MJ, Thomson C, et al. mito-QC illuminates mitophagy and mitochondrial architecture in vivo. *Journal of Cell Biology.* 2016;214(3):333-45.
48. Ayala-Torres S, Chen YM, Svoboda T, Rosenblatt J, and Van Houten B. Analysis of gene-specific DNA damage and repair using quantitative polymerase chain reaction. *Methods.* 2000;22(2):135-47.
49. Hombrebueno JR, Luo C, Guo LD, Chen M, and Xu HP. Intravitreal Injection of Normal Saline Induces Retinal Degeneration in the C57BL/6J Mouse. *Transl Vis Sci Techn.* 2014;3(2).
50. Albert-Fort M, Hombrebueno JR, Pons-Vazquez S, Sanz-Gonzalez S, Diaz-Llopis M, and Pinazo-Duran MD. Retinal neurodegenerative changes in the adult insulin receptor substrate-2 deficient mouse. *Experimental eye research.* 2014;124:1-10.
51. Limb GA, Salt TE, Munro PM, Moss SE, and Khaw PT. In vitro characterization of a spontaneously immortalized human Muller cell line (MIO-M1). *Investigative ophthalmology & visual science.* 2002;43(3):864-9.
52. Li Q, Lau A, Morris TJ, Guo L, Fordyce CB, and Stanley EF. A syntaxin 1, Galpha(o), and N-type calcium channel complex at a presynaptic nerve terminal: analysis by quantitative immunocolocalization. *The Journal of neuroscience : the official journal of the Society for Neuroscience.* 2004;24(16):4070-81.

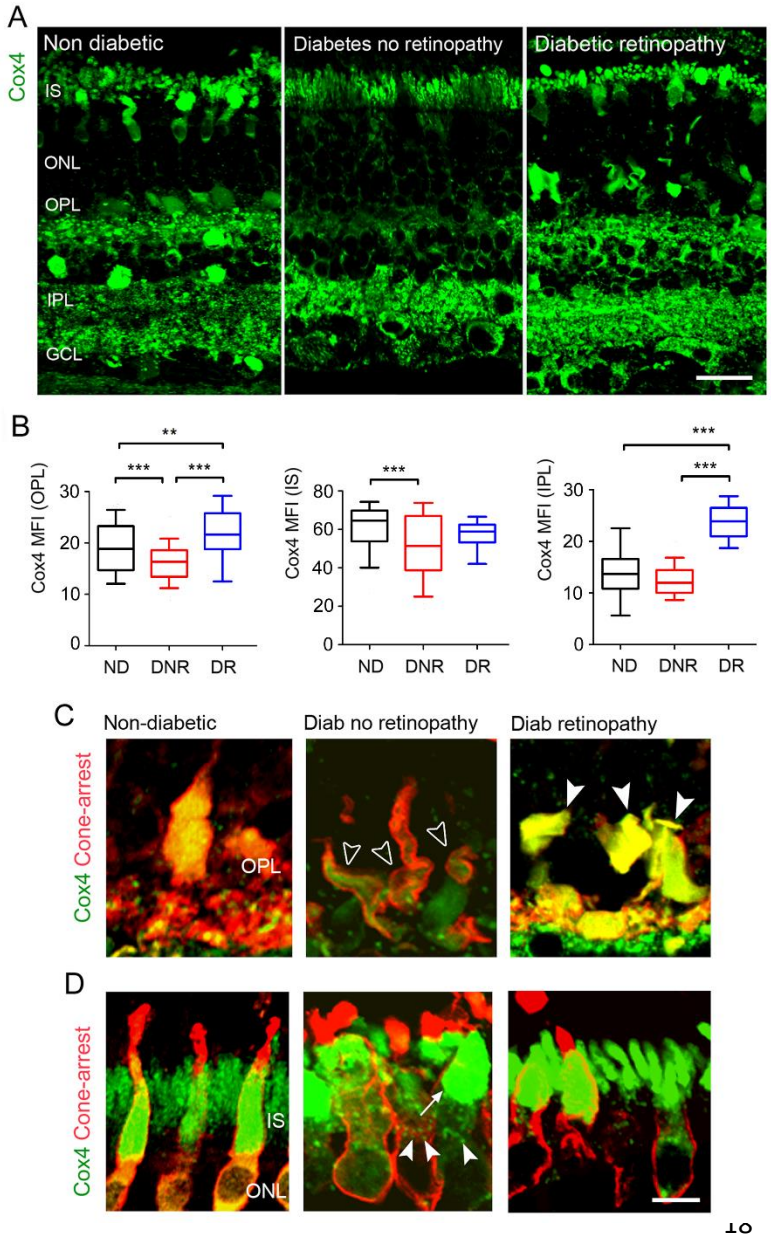

Fig 1. Cox4^{+} mitochondrial contents shift during the progression of diabetes in human retinas. (A) Retinal micrographs of human retinas from non-diabetic (ND), diabetic with no retinopathy (DNR) and diabetic retinopathy (DR) individuals processed for Cox4 immunostaining. (B) The mean fluorescence intensities (MFI) of Cox4 in photoreceptor IS, OPL and IPL of ND (n=3 eyes), DNR (n=5 eyes) and DR (n=2 eyes) individuals (n=16 technical replicates per donor eye were used). Data is presented in box-and-whisker plots. (C-D) Retinal micrographs from ND, DNR and DR individuals processed for Cox4 and cone-arrestin immunostaining in (C) photoreceptor synaptic terminals and (D) photoreceptor IS. (C) Loss (open arrowheads) and gain (arrowheads) of mitochondrial contents in cone-photoreceptor synaptic terminals. (D) Redistribution (arrow) and fragmentation (arrowheads) of Cox4^{+} mitochondria in cone-photoreceptor IS. **p<0.01, ***p<0.001. One-way ANOVA with Bonferroni's correction for multiple comparisons. IS, photoreceptor inner segments; ONL, outer nuclear layer; OPL, outer plexiform layer; IPL, inner plexiform layer; GCL, ganglion cell layer. Scale bars = 40μm (A), 10μm (D).

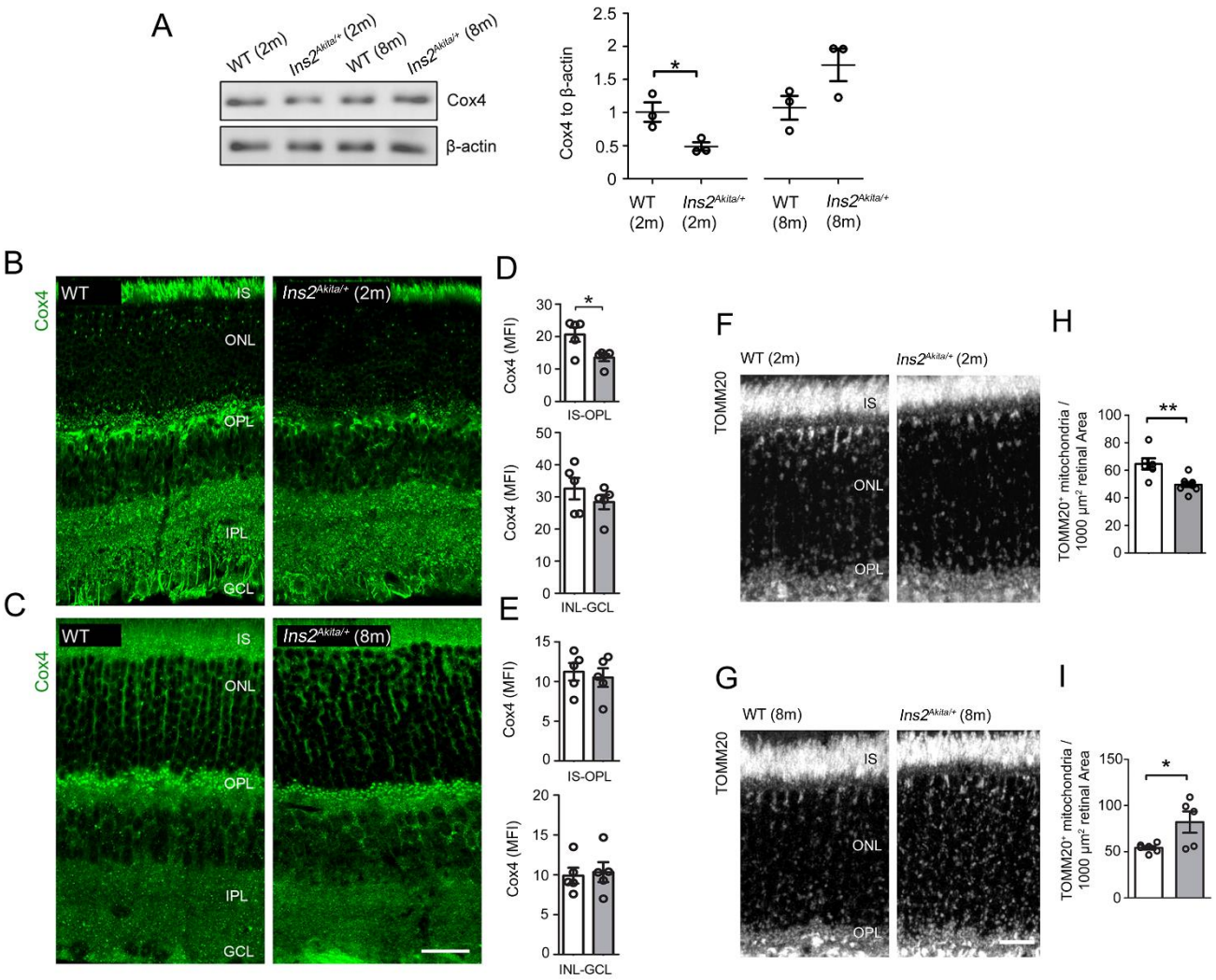

Fig 2. Mitochondrial contents shift during the progression of diabetes in *Ins2*$^{Akita/+}$ mouse retinas. (A) Example immunoblot and quantification of Cox4 in retinal lysates of 2-month and 8-month hyperglycaemic *Ins2*$^{Akita/+}$ and age-matched WT mice. Data was normalized to β-actin loading controls. (B-C) Retinal micrographs of 2-month (B) and 8-month (C) hyperglycaemic *Ins2*$^{Akita/+}$ and age-matched WT mice processed for Cox4 immunostaining. (D-E) The mean fluorescence intensities (MFI) of Cox4 at the IS-OPL and INL-GCL of 2-month (D) and 8-month (E) hyperglycaemic *Ins2*$^{Akita/+}$ and age-matched WT mice. (F-G) Retinal micrographs of 2-month (F) and 8-month (G) hyperglycaemic *Ins2*$^{Akita/+}$ and age-matched WT mice processed for TOMM20 immunostaining. (H-I) The densities of TOMM20^{+} mitochondria at the IS-OPL of 2-month (H) and 8-month (I) hyperglycaemic *Ins2*$^{Akita/+}$ and age-matched WT mice. Keys: WT (white bars), *Ins2*$^{Akita/+}$ (grey bars); n=5-8 eyes per strain. Results presented as mean ± SEM. **p*<0.05, ***p*<0.01, two-sided unpaired Student's *t*-test. IS, photoreceptor inner segments; ONL, outer nuclear layer; OPL, outer plexiform layer; IPL, inner plexiform layer; GCL, ganglion cell layer. Scale bar = 40µm (C), 20µm (G).

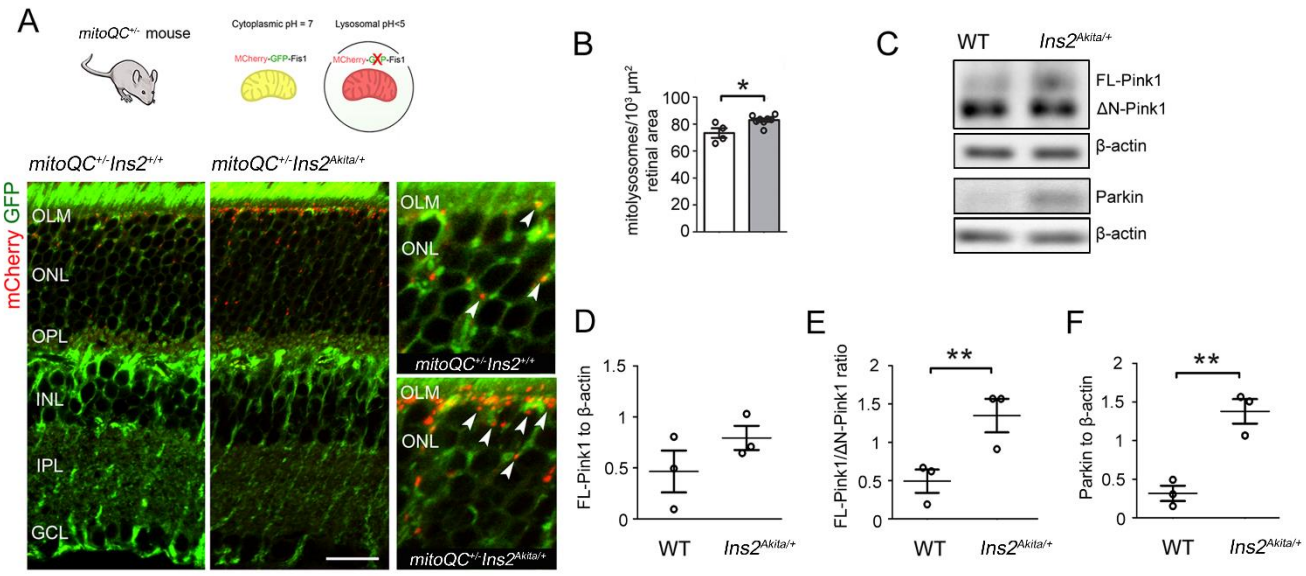

Fig 3. Increased mitophagy at the outer retina of 2-month hyperglycaemic *Ins2$^{Akita/+}$* mice. (A) Confocal photomicrographs showing mitolysosomes (mCherry-only foci – arrowheads) at the IS-OPL of 2-month hyperglycaemic mitophagy reporter mice (*mitoQC$^{+/-}$Ins2$^{Akita/+}$*) and non-diabetic siblings (*mitoQC$^{+/-}$Ins2$^{+/+}$*). (B) Mitolysosome density at the IS-OPL. (C) Example immunoblot and (D-F) quantification of Pink1-dependent mitophagy proteins in retinal lysates of 2-month hyperglycaemic *Ins2$^{Akita/+}$* and age-matched WT mice. Data was normalized to β-actin loading controls. Keys (B): *mitoQC$^{+/-}$Ins2$^{+/+}$* (white bars), *mitoQC$^{+/-}$Ins2$^{Akita/+}$* (grey bars); n=3-7 eyes per strain. Results presented as mean ± SEM. *p<0.05, **p<0.01, two-sided unpaired Student's t-test. IS, photoreceptor inner segments; OLM, outer limiting membrane, ONL, outer nuclear layer; OPL, outer plexiform layer; INL, inner nuclear layer; IPL, inner plexiform layer; GCL, ganglion cell layer. Scale bar = 40µm

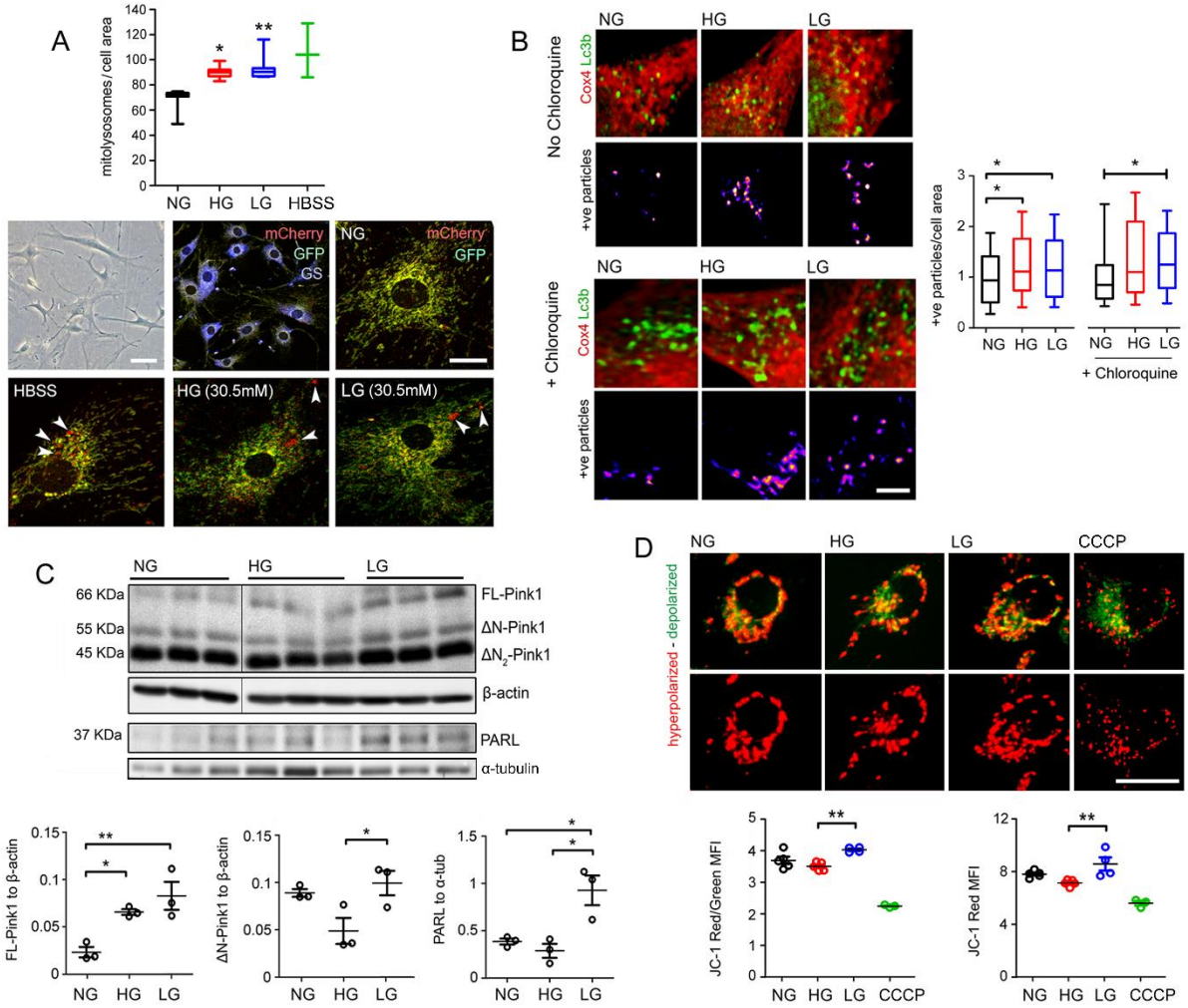

Fig 4. The diabetic milieu dysregulates mitophagy in primary Müller and MIO-M1 cultures *in vitro*. (A) Primary retinal Müller cells isolated from *mitoQC*$^{+/+}$ mouse (*mitoQC*-PMCs) or (B-D) human MIO-M1 cells were maintained for 5 days in normal glucose (NG - 5.5mM), high glucose (HG - 30.5mM) or L-glucose (LG - 30.5mM) osmotic control. (A) *mitoQC*-PMCs had a flattened-elongated shape (bright-field image) and were positive for glutamine synthase (GS) immunoreactivity. Mitolysosome (mCherry-only foci - arrowheads) density was evaluated as index of mitophagy-flux. HBBS (aminoacid starvation - 16h); Data is presented in box-and-whisker plots, n=3-5 biological replicates per group. (B) Quantification of Cox4/Lc3b co-localizing particles in different treatment groups ± 100μM chloroquine for final 16 h of treatment. Data presented as fold-change vs NG control cells in box-and-whisker plots; at least 70 cells, obtained from n=3 biological replicates per group. (C) Example immunoblot and quantification of Pink1-dependent mitophagy proteins in different treatment groups. Data was normalized to β-actin or α-tubulin loading controls; n=3 biological replicates per group. Pink1 lanes and corresponding β-actin loading controls were run on the same gel but were non-contiguous (D) Evaluation of mitochondrial membrane potential by JC-1 dye (red - hyperpolarized mitochondria; green - depolarized mitochondria) in different treatment groups. CCCP (20 μM) was added as a mitochondrial uncoupler positive control (16h); n=3-4 biological replicates per group. Results presented as mean ± SEM in A, C-D. *p<0.05, **p<0.01. One-way ANOVA with Bonferroni's correction for multiple comparisons; HBBS,

Hanks' Balanced Salt solution; MFI, mean fluorescence intensity. Scale bar = 100μm (A, brightfield), 20μm (A, Mcherry-GFP, D), 2μm (B).

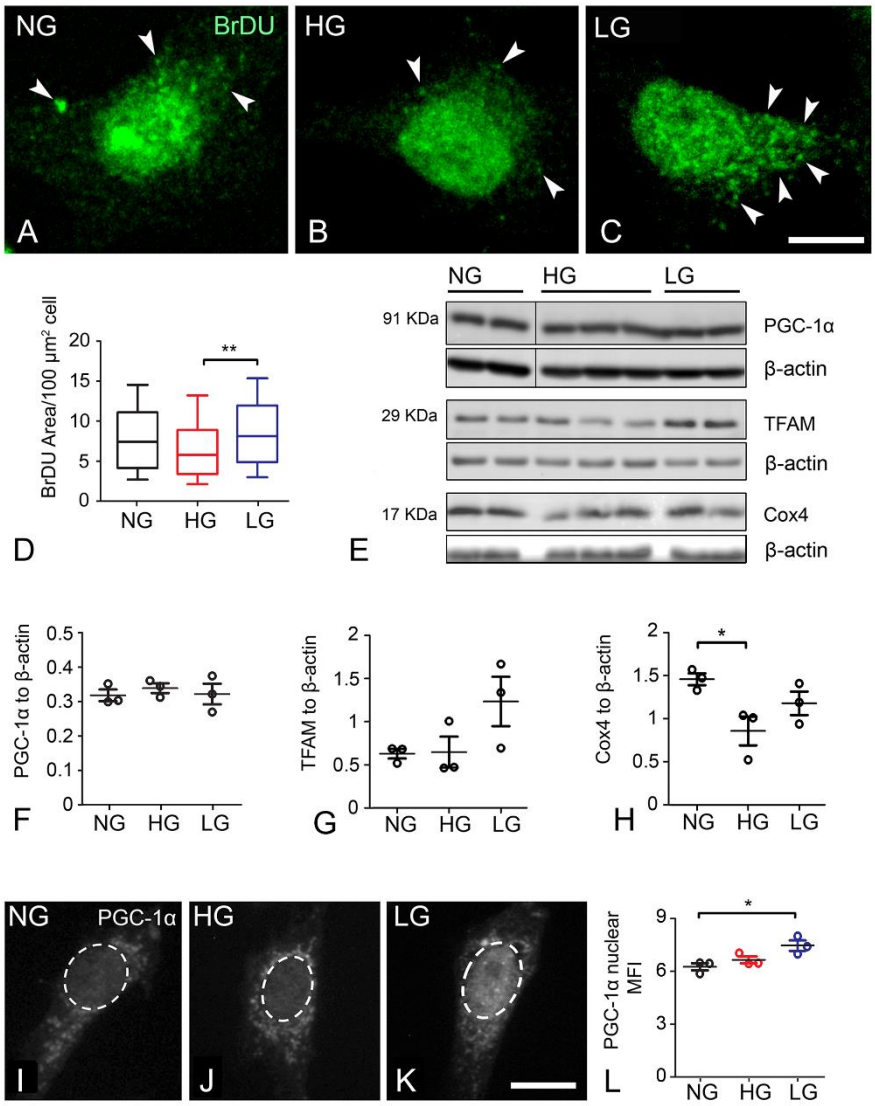

Fig 5. The diabetic milieu dysregulates mitochondrial biogenesis in MIO-M1 cultures *in vitro*. MIO-M1 cells were maintained for 5 days in normal glucose (NG - 5.5mM), high glucose (HG - 30.5mM) or L-glucose (LG - 30.5mM) osmotic control. (A-C) Representative confocal micrographs and (D) quantification of mitochondrial biogenesis by incorporation of Bromodeoxyuridine (BrDU) into mtDNA (arrowheads) in different treatment groups; data is presented in box-and-whisker plots; at least 70 cells, obtained from n=3 biological replicates per group. (E) Example immunoblot and (F-H) quantification of mitochondrial biogenesis proteins in different treatment groups. Data was normalized to β-actin loading control; n=3 biological replicates per group. PGC-1α lanes and corresponding β-actin loading controls were run on the same gel but were non-contiguous. PGC-1α shared similar β-actin loading controls to those in Fig 4C (Pink1). (I-K) Representative confocal micrographs of PGC-1α immunostaining in different treatment groups. (L) Quantification of nuclear PGC-1α mean fluorescence intensity (MFI) in different treatment groups; n=3 biological replicates per group. Results presented as mean ± SEM in F-H, L. *p<0.05, **p<0.01. One-way ANOVA with Bonferroni's correction for multiple comparisons. Scale bars = 10µm.

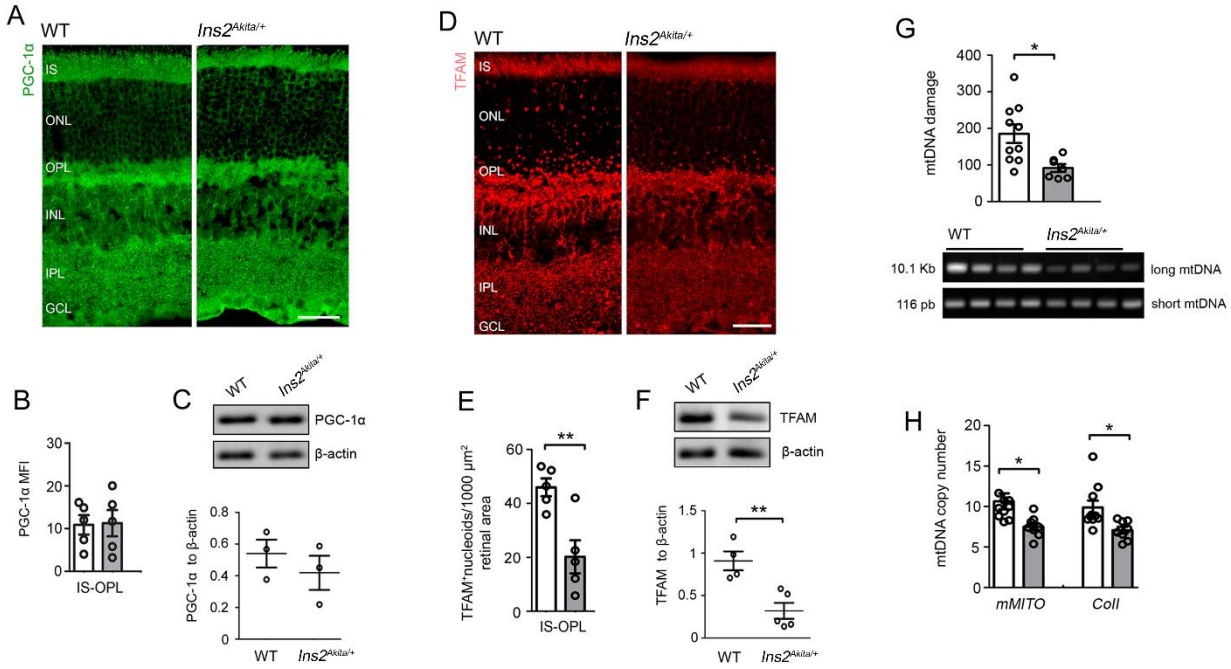

Fig 6. Impairment of mitochondrial biogenesis machinery in 8-month hyperglycaemic *Ins2*$^{Akita/+}$ mouse retinas. (A) Retinal micrographs from 8-month hyperglycaemic *Ins2*$^{Akita/+}$ and aged-matched WT mice processed for PGC-1α immunostaining. (B) The mean fluorescence intensity (MFI) of PGC-1α at the IS-OPL. (C) Example immunoblot and quantification of PGC-1α in mouse retinal lysates of 8-month hyperglycaemic *Ins2*$^{Akita/+}$ and age-matched WT. (D) Retinal micrographs from 8-month hyperglycaemic *Ins2*$^{Akita/+}$ and aged-matched WT mice processed for TFAM immunostaining. (E) The density of TFAM^{+} mitochondrial nucleoids at the IS-OPL. (F) Example immunoblot and quantification of TFAM in mouse retinal lysates of 8-month hyperglycaemic *Ins2*$^{Akita/+}$ and age-matched WT. Data was normalized to β-actin loading controls. TFAM shared similar β-actin loading controls to those in Fig 2A (Cox4). (G) Evaluation of mtDNA damage in 8-month hyperglycaemic *Ins2*$^{Akita/+}$ and age-matched WT mouse retinas by amplification of long (10.1Kb) and short (116pb) mtDNA regions. A reduction in the long/short amplification ratio is indicative of mtDNA damage. (H) Mitochondrial copy numbers evaluated by rtPCR analysis of *mMITO* and *CoII* mtDNA regions. Keys: WT (white bars), *Ins2*$^{Akita/+}$ (grey bars); n=3-10 eyes per strain. (F). Results presented as mean ± SEM. **p*<0.05, ***p*<0.01, two-sided unpaired Student's *t*-test. IS, photoreceptor inner segments; ONL, outer nuclear layer; OPL, outer plexiform layer; INL, inner nuclear layer; IPL, inner plexiform layer; GCL, ganglion cell layer. Scale bars = 40µm.

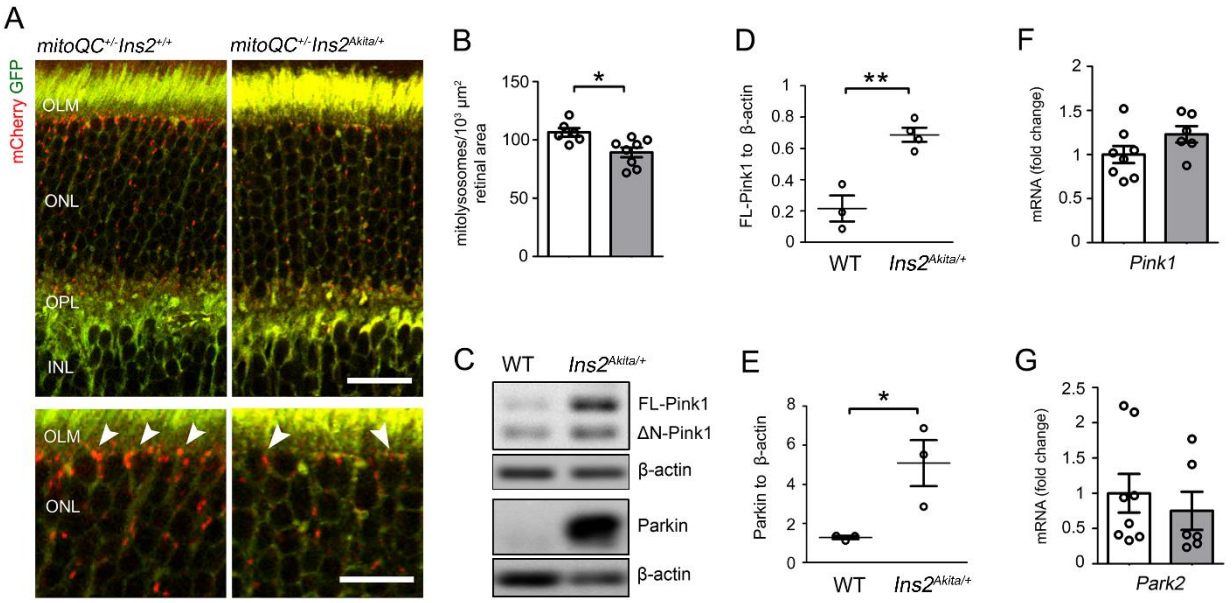

Fig 7. Mitophagy is decreased at the outer retina of 8-month hyperglycaemic *Ins2$^{Akita/+}$* mice. (A) Confocal photomicrographs showing mitolysosomes (mCherry-only foci – arrowheads) at the IS-OPL of 8-month hyperglycaemic mitophagy reporter mice (*mitoQC$^{+/-}$Ins2$^{Akita/+}$*) and non-diabetic siblings (*mitoQC$^{+/-}$Ins2$^{+/+}$*). (B) Mitolysosome density at the IS-OPL. (C) Example immunoblot and quantification (D-E) of Pink1-dependent mitophagy proteins in retinal lysates of 8-month hyperglycaemic *Ins2$^{Akita/+}$* and age-matched WT mice. Data was normalized to β-actin loading controls. (F-G) rtPCR analysis of *Pink1* and *Park2* gene transcripts in the retina of 8-month hyperglycaemic *Ins2$^{Akita/+}$* and age-matched WT mice. Keys (B): *mitoQC$^{+/-}$Ins2$^{+/+}$* (white bars), *mitoQC$^{+/}$ Ins2$^{Akita/+}$* (grey bars); Keys (F-G): WT (white bars), *Ins2$^{Akita/+}$* (grey bars); n=3-8 eyes per strain. Results presented as mean ± SEM. *p<0.05, **p<0.01, two-sided unpaired Student's *t*-test. IS, photoreceptor inner segments; OLM, outer limiting membrane; ONL, outer nuclear layer; OPL, outer plexiform layer; INL, inner nuclear layer. Scale bars = 40µm (A), 20µm (inset in A).

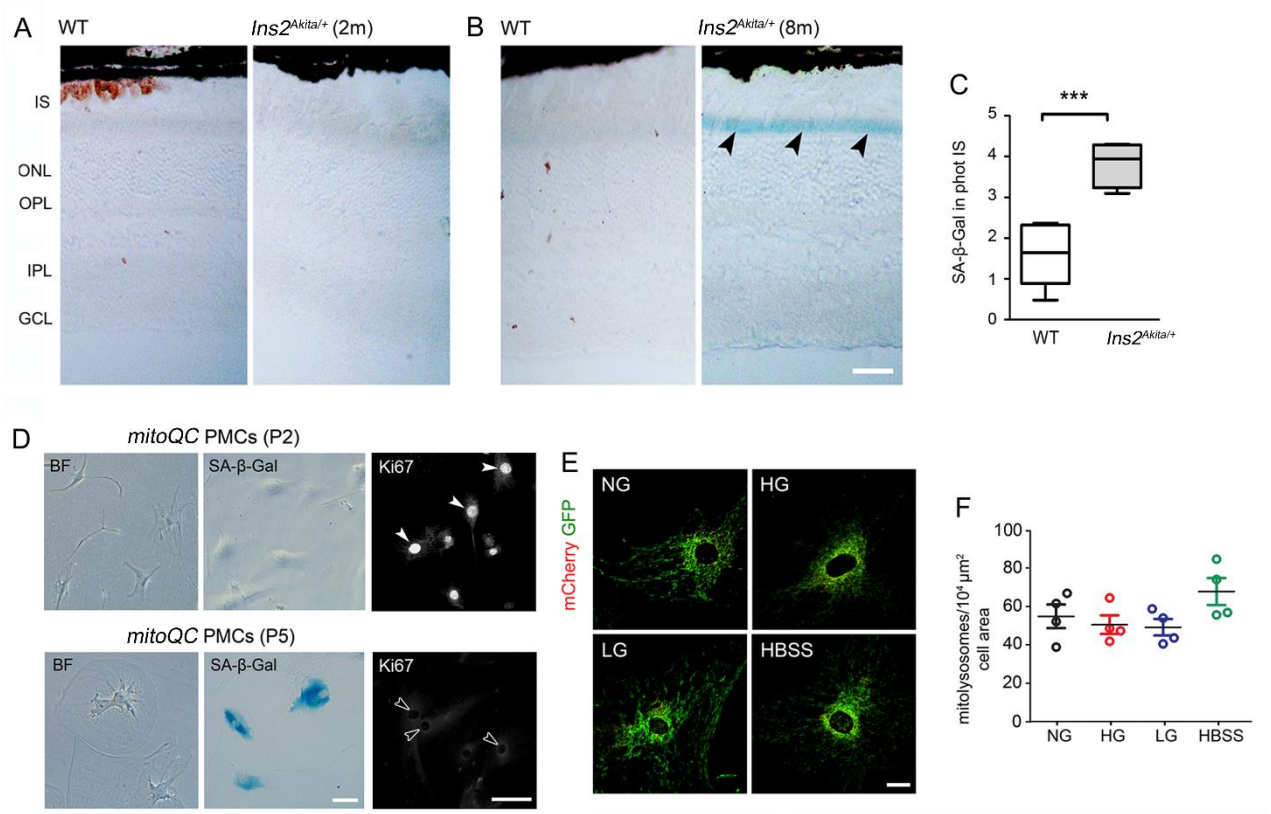

Fig 8. Senescence in the diabetic retina may disrupt mitochondrial quality control. (A, B) Retinal micrographs from 2-month (A) and 8-month (B) hyperglycaemic *Ins2*$^{Akita/+}$ and aged-matched WT mice processed for SA-β-Gal activity. Increased SA-β-Gal activity in photoreceptor IS of 8-month hyperglycaemic *Ins2*$^{Akita/+}$ mice (arrowheads). (C) The levels of SA-β-Gal activity in photoreceptor IS in 8-month hyperglycaemic *Ins2*$^{Akita/+}$ and aged-matched WT. Data are presented in box-and-whisker plots; n=6 eyes per group. (D) Brightfield (BF) images of primary retinal Müller cells isolated from *mitoQC*$^{+/+}$ mouse (*mitoQC*-PMCs) showing their morphology, SA-β-Gal activity and Ki67 immunostaining at passage (P)2 and P5. Proliferative non-senescent *mitoQC*-PMCs show high nuclear-levels of Ki67 (P2 - arrowheads), in contrast to senescent cultures (P5 - open arrowheads). (E, F) Mitolysosome (mCherry-only foci) density was quantified (F) in P5-P6 *mitoQC* PMCs maintained for 5 days in normal glucose (NG - 5.5mM), high glucose (HG - 30.5mM) or L-glucose (LG - 30.5mM) osmotic control. HBBS (aminoacid starvation - 16h); n=2 biological replicates and 4 technical replicates per group. Results are presented as mean ± SEM. ***p<0.001, two-sided unpaired Student's t-test in (C); One-way ANOVA with Bonferroni's correction for multiple comparisons in (F). IS, photoreceptor inner segments; ONL, outer nuclear layer; OPL, outer plexiform layer; INL, inner nuclear layer; IPL, inner plexiform layer; GCL, ganglion cell layer. HBBS, Hanks' Balanced Salt solution; Scale bars = 40µm (B), 20µm (D, E).